Int. J. Heat Mass Transfer. Vol. 37, No. 2, pp. 303–312, 1994
Printed in Great Britain

0017–9310/94 $6.00 + 0.00

Natural convection in a finite wall rectangular cavity filled with an anisotropic porous medium

WEN-JENG CHANG
Department of Mechanical Engineering, Feng Chia University, Taichung, Taiwan, R.O.C.

and

HUI-CHUAN LIN
Aeronautic Research Laboratory, Chung Shan Institute of Science Technology, Taichung, Taiwan, R.O.C.

(*Received* 4 *May* 1993)

Abstract—A numerical study has been made to analyze the wall conduction effect on the natural convection in an anisotropic fluid-saturated porous medium filled in a rectangular cavity. The governing conservation equations are solved by a SIMPLE algorithm. The numerical results indicate that the anisotropic permeability influences the flow field and heat transfer rate significantly. A critical value of the anisotropic thermal diffusivity ratio may exist such that the Nusselt number reaches a minimum. This critical value decreases with increasing the value of the anisotropic permeability ratio. Moreover, wall conductance effect can lead to large changes in the Nusselt numbers.

1. INTRODUCTION

NATURAL convection in a porous medium has been studied extensively over the past twenty years due to the numerous application in geophysics, oil recovery techniques, thermal insulation engineering, packed-bed catalytic reactors, and heat storage beds. Excellent reviews are available [1–3]. So far, the investigations have usually been concerned with isotropic porous media. The natural convection in a rectangular cavity filled with an isotropic porous medium has been studied and reported in the literature [4–8]. However, many porous materials are anisotropic, for example, fibrous medium presents a form of anisotropy. Another important example is groundwater motion in sediments and other anisotropic rocks, especially in areas with geothermal activity. Kvernvold and Tyvand [9] and Bories [10] studied the effect of anisotropy on the criterion for the onset of convection in a horizontal porous layer. Burns *et al.* [11] incorporated anisotropic permeability in their study of convection in vertical slots.

The reported studies dealing with natural convection in a porous cavity have considered the interaction between convection in the fluid-filled porous media and conduction of heat of obstruction are limited to the partitioned porous enclosure. Bejan and Anderson [12] demonstrated that the insert of a vertical impermeable partition reduces significantly the net heat transfer rate through the layer. Bejan [13] examined the effect of centrally-located internal obstruction on heat transfer through a two-dimensional porous layer heated from the side. Three types of flow obstruction were considered: horizontal diathermal partition, horizontal adiabatic partition and vertical diathermal partition. Tong and Subramanian [14] and Beckermann *et al.* [15] investigated the natural convection in a rectangular enclosure, vertically divided into a region filled with a fluid and another filled with a fluid-saturated porous media. In addition, Kim and Viskanta [16] showed that the thermal boundary condition (wall conductance) could lead to significant changes in the convective heat transfer coefficient for a viscous fluid in an enclosure. However, the studies have neglected the interaction between convection in the fluid-filled porous cavity and conduction of heat in the walls forming the enclosure by using idealized boundary conditions such as those corresponding to a prescribed temperature or heat flux. The wall conductance and anisotropic effects in a porous cavity seem not to have been investigated. This has motivated the present investigation.

The purpose of this paper is to examine analytically the effects of wall heat conduction and anisotropy on natural convection in an anisotropic fluid-saturated porous medium filled in a rectangular cavity having finite wall conductances. Since there are many governing parameters in such a problem only the square cavity is considered in this study, and the vertical and the horizontal walls are assumed to be of the same material. The results will provide useful information for the storage of agricultural products, insulation problems and nuclear engineering. The left and right of the outside vertical walls of the porous cavity are imposed constant but different temperature, while the horizontal connecting walls are assumed to be insulated on the outside. The anisotropy in the permeability and in the thermal diffusivity is considered. The resulting governing equations are solved by using the SIMPLE algorithm.

NOMENCLATURE

AR	anisotropic thermal diffusivity ratio
g	gravitational acceleration
h	height of the porous cavity
H	height of the enclosure
k	thermal conductivity
K	permeability
K^*	anisotropic permeability ratio
l	height of the porous cavity
L	height of enclosure
Nu	local Nusselt number
$\overline{Nu}$	average Nusselt number
P	pressure
Ra^*	Darcy modified Rayleigh number
T	temperature
u, v	velocity component in x, y directions
U, V	dimensionless velocity in x, y directions
x, y	horizontal and vertical coordinates
X, Y	dimensionless coordinates.

Greek symbols

α	thermal diffusivity
β	thermal expansion coefficient
θ	dimensionless temperature, $(T-T_c)/(T_h-T_c)$
μ	viscosity of fluid
ρ	density of fluid.

Subscripts

c	cold
h	hot
w	wall
x	x direction
y	y direction.

2. ANALYSIS

The physical situation and coordinate system are shown in Fig. 1. The rectangular porous cavity is formed by walls having finite conductance. The vertical and the horizontal walls are assumed to be of the same material. The left and right of the outside vertical walls of the porous cavity are imposed constant but different temperatures. The horizontal connecting walls are assumed to be insulated on the outside. The flow is assumed to be two dimensional. The fluid in the porous cavity is assumed to have constant properties except in so far as the buoyancy is concerned, the convecting fluid and the porous matrix are in local thermodynamic equilibrium. Darcy's law and the Boussinesq approximations are employed.

Then, the equations that account for the conservation of mass, momentum, and energy for the porous cavity are as follows.

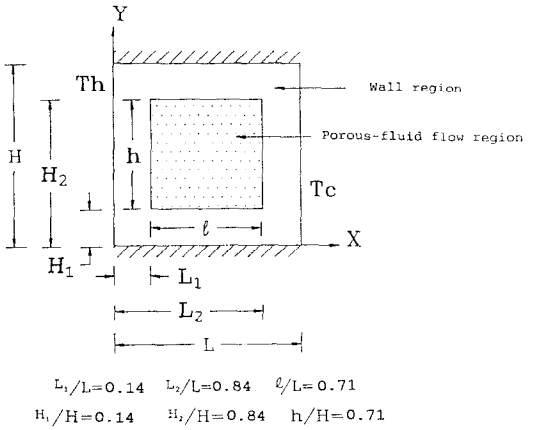

FIG. 1. The physical situation and coordinate system.

$$\frac{\partial u}{\partial x}+\frac{\partial v}{\partial y}=0 \tag{1}$$

$$u=-\frac{K_x}{\mu}\frac{\partial p}{\partial x} \tag{2}$$

$$v=-\frac{K_y}{\mu}\left[\frac{\partial p}{\partial y}-\rho g\beta(T-T_c)\right] \tag{3}$$

$$u\frac{\partial T}{\partial x}+v\frac{\partial T}{\partial y}=\alpha_x\frac{\partial^2 T}{\partial x^2}+\alpha_y\frac{\partial^2 T}{\partial y^2} \tag{4}$$

and for the walls:

$$\frac{\partial^2 T_w}{\partial x^2}+\frac{\partial^2 T_w}{\partial y^2}=0 \tag{5}$$

where the subscript w signifies the walls quantities; K_x and K_y are the x-direction and y-direction permeability of the saturated porous medium, respectively; and α_x and α_y are the x-direction and y-direction thermal diffusivity, respectively. The other various symbols are defined in the Nomenclature.

The temperature boundary conditions at the interior walls of the enclosure are

$$Q=-k\frac{\partial T}{\partial n}=-k_w\frac{\partial T_w}{\partial n} \tag{6}$$

where n represents x or y.

The temperature boundary conditions on the outside walls of the enclosure are

$$x=0,\ T_w=T_h;\ x=L,\ T_w=T_c$$

$$y=0,\ \frac{\partial T_w}{\partial y}=0;\ y=H,\ \frac{\partial T_w}{\partial y}=0. \tag{7}$$

The boundary conditions for the velocity on the surface bounding the porous cavity are

$$x = L_1,\ u = 0;\ x = L_2,\ u = 0$$
$$y = H_1,\ v = 0;\ y = H_2,\ v = 0. \quad (8)$$

The following dimensionless variables are introduced

$$X = \frac{x}{L},\ Y = \frac{y}{L},\ U = \frac{uL}{\alpha_x},\ V = \frac{vL}{\alpha_x},\ P = \frac{pk_x}{\alpha_x \mu}$$
$$\theta = \frac{T - T_c}{T_h - T_c},\ K^* = \frac{K_y}{K_x},\ AR = \frac{\alpha_y}{\alpha_x},$$
$$KR = \frac{k_w}{k};\ Ra^* = \frac{LK_y g\beta(T_h - T_c)}{\alpha_x \nu}. \quad (9)$$

Then, equations (1)–(5) become

for the porous cavity:

$$\frac{\partial U}{\partial X} + \frac{\partial V}{\partial Y} = 0 \quad (10)$$

$$U = -\frac{\partial P}{\partial X} \quad (11)$$

$$V = -K^* \frac{\partial P}{\partial Y} + Ra^* \cdot \theta \quad (12)$$

$$U\frac{\partial \theta}{\partial X} + V\frac{\partial \theta}{\partial Y} = \frac{\partial^2 \theta}{\partial X^2} + AR\frac{\partial^2 \theta}{\partial Y^2} \quad (13)$$

for the walls:

$$\frac{\partial^2 \theta_w}{\partial X^2} + \frac{\partial^2 \theta_w}{\partial Y^2} = 0 \quad (14)$$

with the dimensionless boundary conditions

$$X = \frac{L_1}{L},\ U = 0,\ \theta = \theta_w,\ \frac{\partial \theta}{\partial X} = KR\frac{\partial \theta_w}{\partial X}$$
$$Y = \frac{L_2}{L},\ U = 0,\ \theta = \theta_w,\ \frac{\partial \theta}{\partial X} = KR\frac{\partial \theta_w}{\partial X}$$
$$Y = \frac{H_1}{L},\ V = 0,\ \theta = \theta_w,\ \frac{\partial \theta}{\partial Y} = KR\frac{\partial \theta_w}{\partial Y}$$
$$Y = \frac{H_2}{L},\ V = 0,\ \theta = \theta_w,\ \frac{\partial \theta}{\partial Y} = KR\frac{\partial \theta_w}{\partial Y}$$
$$X = 0,\ \theta_w = 1$$
$$X = 1,\ \theta_w = 0$$
$$Y = 0,\ \frac{\partial \theta_w}{\partial Y} = 0$$
$$Y = 1,\ \frac{\partial \theta_w}{\partial Y} = 0. \quad (15)$$

When $K^* = AR = 1$, equations (10)–(15) reduced to the isotropic porous medium with isotropic thermal diffusivity, and as $KR = 1$, the bulk thermal conductivity of the saturated porous medium is equal to that of the wall materials.

In terms of new variables, it can be shown that the local and average Nusselt numbers are given by

$$Nu_X = -\frac{\partial \theta}{\partial Y} \cdot AR\Big|_{Y = H_1/L,\ H_2/L}$$
$$Nu_Y = -\frac{\partial \theta}{\partial X}\Big|_{X = L_1/L,\ L_2/L}$$

and

$$\overline{Nu_X} = \frac{1}{1/L}\int Nu_X \,dX$$
$$\overline{Nu_Y} = \frac{1}{h/L}\int Nu_Y \,dY. \quad (16)$$

3. NUMERICAL METHOD OF SOLUTION

A conventional numerical scheme with nonuniform (33 × 33) grids, as shown in Fig. 2, was applied to the present physical system. The finest grid, of size 0.01, is located adjacent to the wall.

The numerical procedure used is based on the iterative scheme. The hybrid central/upwind differences is used for the convective terms with central difference for the diffusion terms. For the convective term, upwind differencing is used if the grid Peclet number in a given direction is greater than or equal to 2. Otherwise, central differences are employed. This procedure incorporates the SIMPLE solution technique initiated by Patankar [17], which is based on the solution of difference equations obtained by integrating the differential equations for momentum and energy over control volumes enclosing the nodal points. The set of difference equations is solved over the entire region of interest by obtaining new values for any desired variable by taking into account the latest known estimated value of that variable on the neighboring nodes. One iteration of the solution is complete when, in a line by line technique, all the lines in a chosen direction have been accounted for. Line inversion interaction with an under relaxation value of 0.5 for velocity terms, 0.6 for the pressure correction term and 0.8 for the temperature term was incorporated to facilitate calculation.

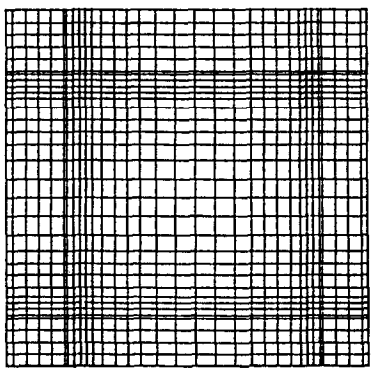

FIG. 2. Non-uniform grid system.

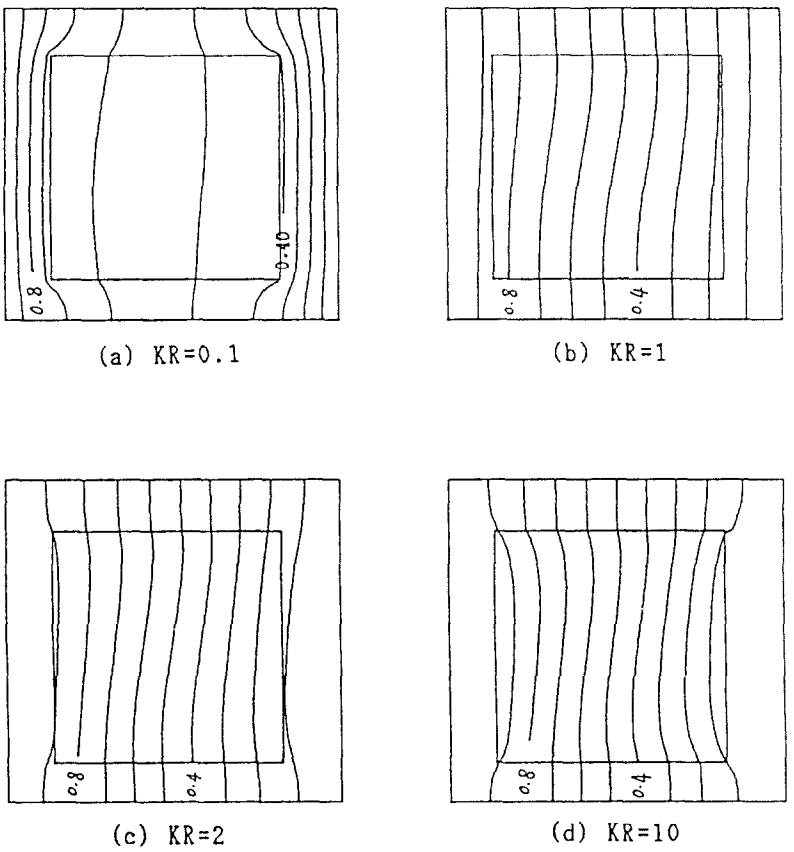

FIG. 3. The contours of isotherm for (a) $KR = 0.1$, (b) $KR = 1$, (c) $KR = 2$, (d) $KR = 10$ ($Ra^* = 10$, $K^* = 1$, $AR = 1$, $LH = 1$).

By first assuming a pressure distribution within the pressure cavity domain, the set of difference equations for the x- and y-momentum and energy equations for the porous cavity and the walls is solved by line iteration. After a sweep of the solution domain is completed, adjustments are made to the pressure field so that the continuity, momentum, and energy equations are satisfied simultaneously. The convergence criterion adopted is that the change of a variable at any node should be less than 0.0001.

4. RESULT AND DISCUSSIONS

Numerical result for the streamlines, isotherms and the Nusselt number are obtained for $1 \leqslant K^* \leqslant 10$, $1 \leqslant AR \leqslant 10$, $1 \leqslant KR \leqslant 240$, and $1 \leqslant Ra^* \leqslant 500$. These ranges of K^* and AR are the same of those in refs. [10, 18, 19].

Figure 3 shows that the effects of the thermal conductivity ratios (KR) of wall to porous–fluid cavity on the isotherms of the enclosure. It is seen that, as would be expected, the ratio between the temperature gradients of the porous–fluid cavity to the walls increases with increasing value of the KR, and that the inside hot and cold surfaces of the cavity are not isothermal. Note that, the temperature gradients do not vanish at the horizontal top and bottom surfaces of the porous cavity.

Numerical solutions of average Nusselt number vs KR are shown in Fig. 4. for the high temperature side and the bottom side. It is seen that as KR is less than

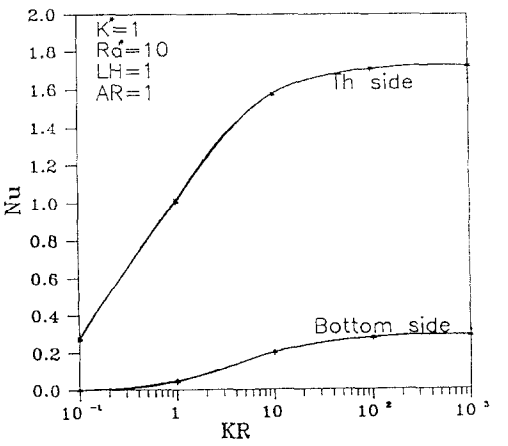

FIG. 4. The local Nusselt number are as function of KR for Th side and bottom side.

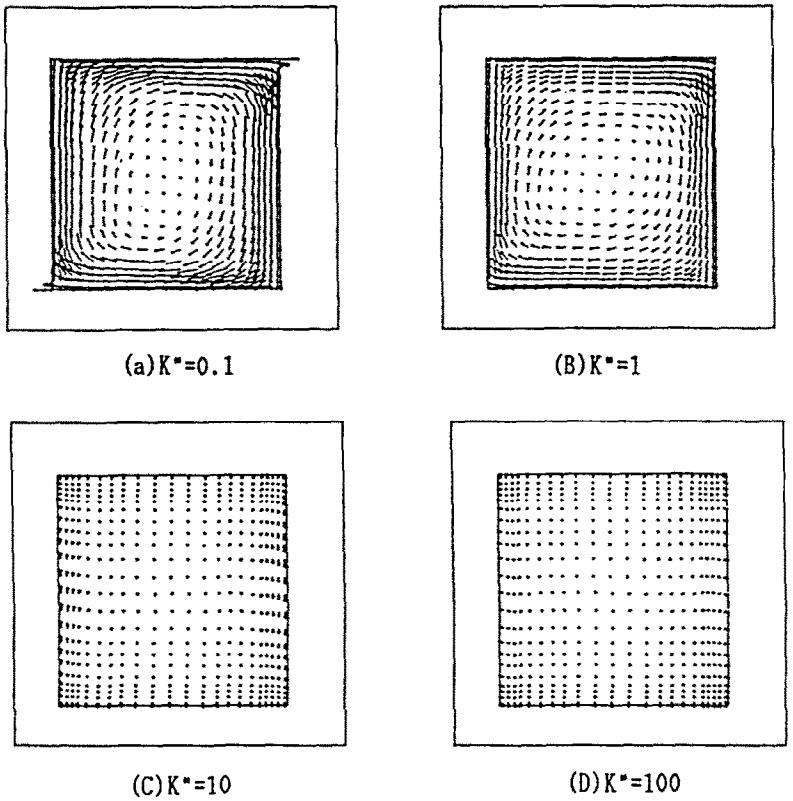

FIG. 5. The velocity field of flow system for different K^* ($Ra^* = 100$, $KR = 240$, $LH = 1$, $AR = 1$).

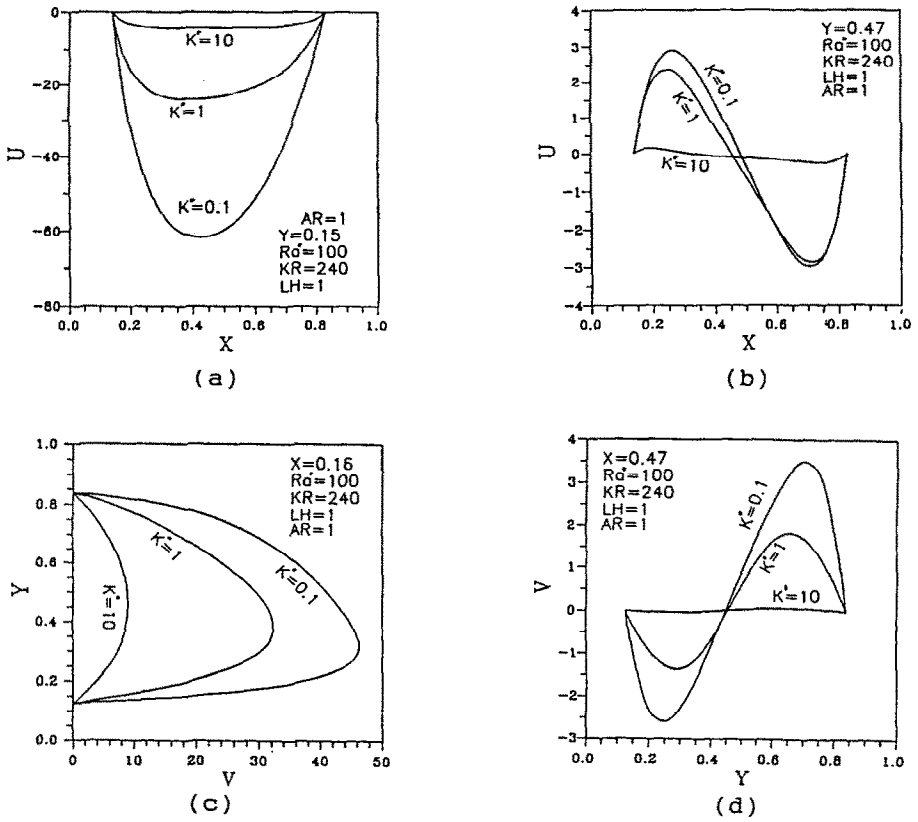

FIG. 6. The velocity distribution at (a) $Y = 0.5$, (b) $Y = 0.47$, (c) $X = 0.16$, (d) $X = 0.47$.

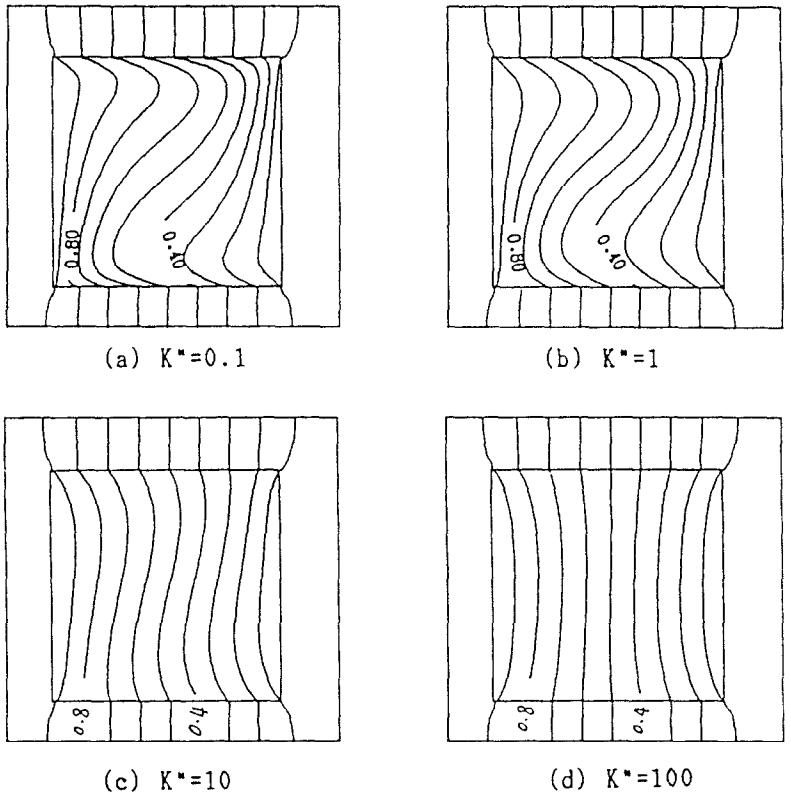

FIG. 7. The contours of isotherms in enclosure for selected values of K^* ($Ra^* = 100$, $KR = 240$, $AR = 1$, $LH = 1$).

100, the average Nusselt number increases significantly; while, as KR is greater than 100, the average Nusselt numbers increases slowly. Thus, wall conduction has a large effect on the Nu calculation. This is primarily due to the fact that the heat conduction in the walls causes the temperature distribution in the insulated (on the outside) walls to be deviated from that of the adiabatic case. Natural convection in the porous cavity can also induce conduction heat transfer in the surrounding walls.

Figure 5 shows the effects of anisotropic permeability on the dimensionless velocity, for $AR = 1$, $Ra^* = 100$, $KR = 240$, $LH = 1$. As $K^* < 1$ (i.e. $K_y < K_x$), the velocity is larger than that of isotropic permeability case ($K^* = 1$); as $K^* > 1$, the velocity is smaller than that of the case of $K^* = 1$. The x-component velocity U vs X are shown in Fig. 6(a) (for $Y = 0.15$), and Fig. 6(b) (for $Y = 0.47$) for three different values of K^*. The y-component velocity V is shown in Fig. 6(c) (for $X = 0.15$) and Fig. 6(d) (for $X = 0.5$). These figures show that as the K^* decreases, the local absolute velocity increases.

Figure 7 gives the isothermal lines for different values of K^*. As $K^* < 1$ the convective effect is stronger than $K^* = 1$; as the value of K^* increases from one, the heat transfer mode changes from convective mode to conduction mode. That is, the Nusselt number decrease with increasing the value of K^*. This phenomenon is more apparent as seen in Figs. 8 and 9. Figure 8 shows the variation of the local Nusselt number with Y at three different values of K^*. It is shown that at the bottom-left corner, as K^* is smaller, Nu_y is larger. This is because the convection mode is stronger, and the horizontal wall transfers more heat

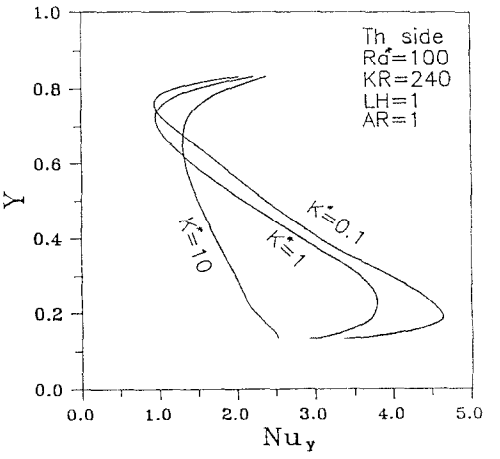

FIG. 8. Nusselt number distributions along the high temperature side-wall of the cavity at different value of K^*.

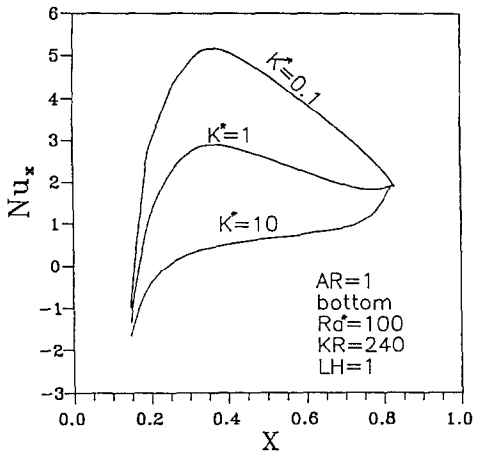

FIG. 9. Nusselt number distributions along the bottom wall of the cavity at different values of K^*.

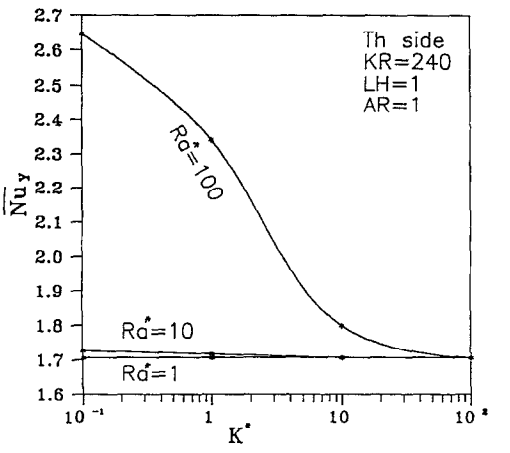

FIG. 10. The average Nusselt number as a function of K^* for different values of Ra^* in the high temperature wall.

to fluid when K^* is smaller. The variations of the local Nusselt number vs X-axis are plotted in Fig. 9.

Figure 10 shows the effects of Rayleigh number and anisotropic permeability on the average Nusselt number. The average Nusselt number increase with increasing value of Ra^*. It is also shown that as the value of K^* increases, the average Nusselt number decreases. The results also indicate that as $K^* > 100$, the effect of Ra^* can be neglected.

It would be interesting to understand the effects of the anisotropic thermal diffusivity. Figures 11 and 12 show the effect of anisotropic permeabilities K^* and

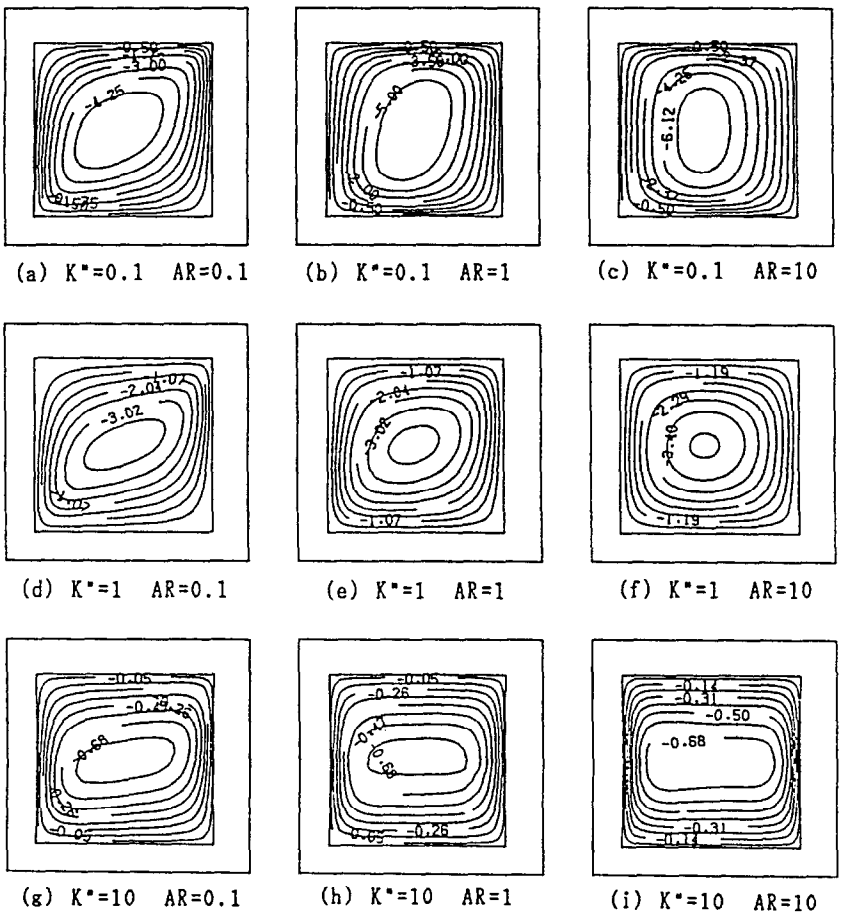

FIG. 11. The contours of streamlines for the different values of K^* and AR ($Ra'' = 100$, $KR = 240$, $LH = 1$).

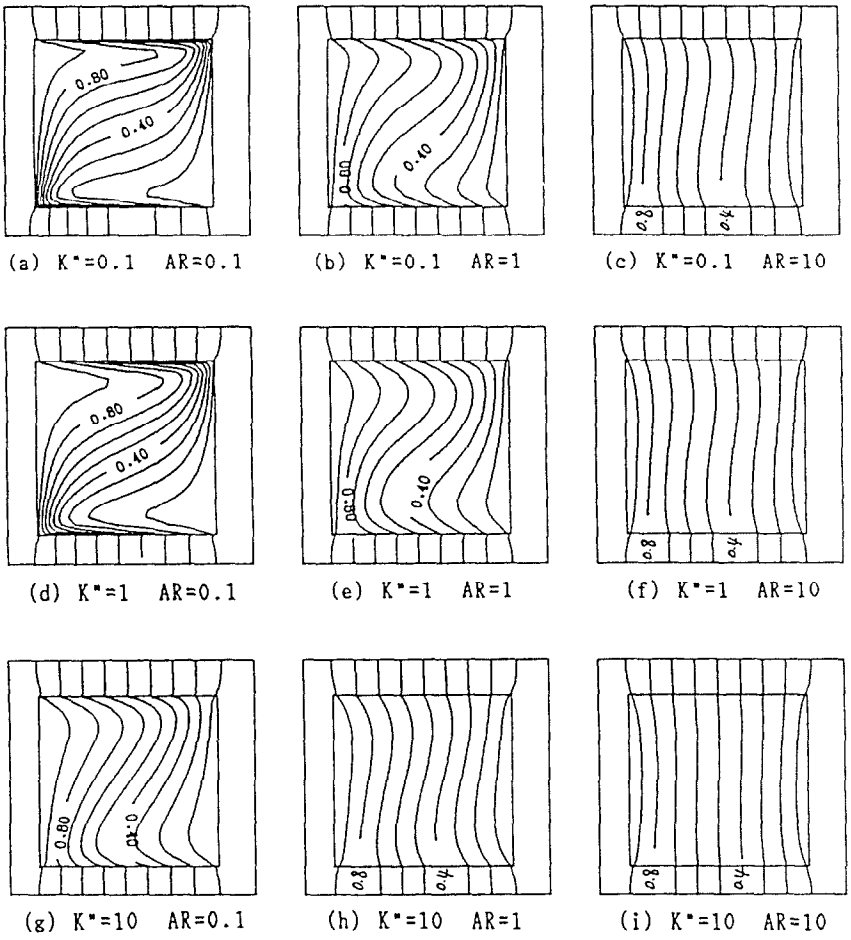

FIG. 12. The contours of isotherm in the enclosure for selected values of K^* and AR ($Ra'' = 100$, $KR = 240$, $LH = 1$).

thermal diffusivities AR on the velocity pattern and isotherms, respectively. Figure 11 shows that the closed streamlines pattern is changed as $AR \neq 1$. Figure 12 shows that the convection is increased with decreasing the values of AR, and the convection is more important as the values of AR and K^* decrease. Figures 13 and 14 show the effects of AR on the local Nusselt numbers at the high temperature side for $K^* = 0.1$ and $K^* = 1$, respectively. The local Nusselt number changes dramatically at the y-direction as the value of AR decreases. Both figures also indicate that as AR decrease, the local Nusselt number in the nearby corner is increasingly influenced by the wall conductance effects. Figure 15 shows the effects of AR on the local Nusselt numbers at the bottom side. It is shown that the local Nusselt number changes more sensitive at the x direction as the value of AR increases.

Numerical solutions of average Nusselt number vs AR for three different K^* values are shown in Figs. 16 and 17 for high temperature side and bottom side, respectively. Figure 16 shows that a critical value of AR exists at which the Nusselt number reaches a minimum. This critical value decreases with increasing the values of K^*. However, this phenomenon is not observed at the bottom side. Both figures indicate that the Nu decreases with increasing the K^* value.

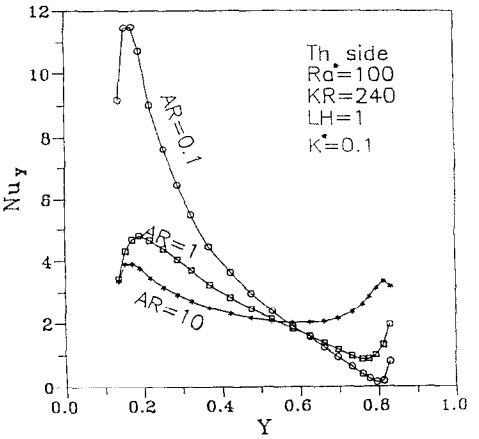

FIG. 13. Nusselt number distributions along the high temperature wall of the cavity at different values of AR for $K^* = 0.1$.

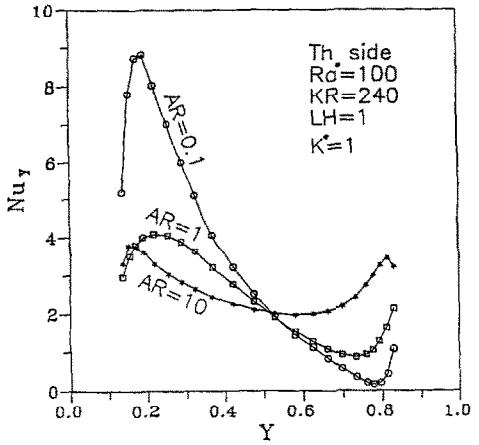

FIG. 14. Nusselt number distributions along the high temperature wall of the cavity at different values of AR for $K^* = 1$.

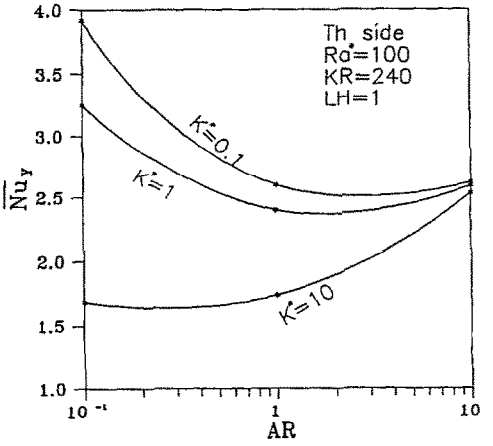

FIG. 16. The average Nusselt number as a function of AR for different value of K^* in the high temperature wall.

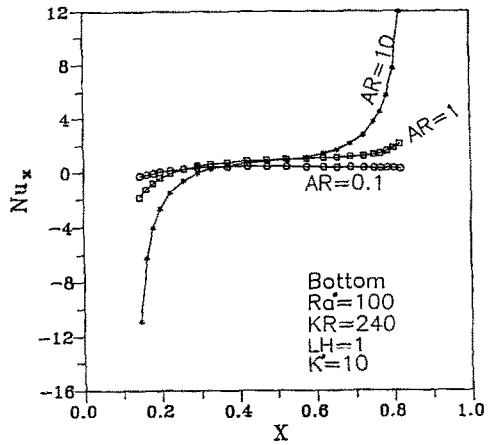

FIG. 15. Nusselt number distributions along the high temperature wall of the cavity at different values of AR for $K^* = 10$.

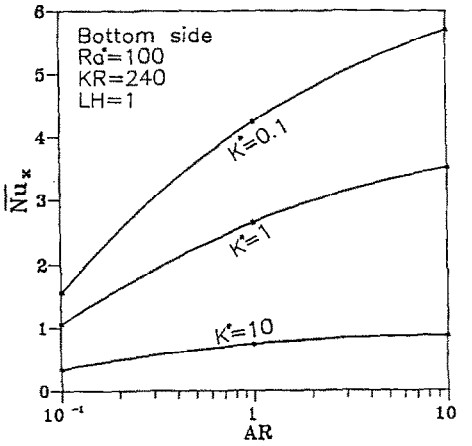

FIG. 17. The average Nusselt number as a function of AR for different value of K^* in the bottom wall.

5. CONCLUSION

The numerical solutions have shown significant effects of anisotropic permeabilities, thermal diffusivity and wall conduction on the convective heat transfer in a rectangular porous cavity. The results indicate that as the ratios of the thermal diffusivity of the walls to porous–fluid cavity (KR) increase, the average Nusselt numbers increase.

The average Nusselt numbers of high temperature side decreases with increasing the value of K^*. A critical value of the anisotropic thermal diffusivity ratio exists at which the Nusselt number reaches a minimum. This critical value decreases which increases the value of the anisotropic permeability ratio.

REFERENCES

1. P. Cheng, Heat transfer in geothermal system, *Adv. Heat Transfer* **14**, 1–105 (1978).
2. P. Cheng, Natural convection in a porous medium: external flows, *NATO Advanced Study Institute on Natural Convection: Fundamentals and Applications*, Izmir, Turkey, 16–27 July (1984).
3. M. A. Combarnous, Natural convection in porous medium and geothermal system, *Proceedings of the 6th International Heat Transfer Conference*, Vol. 6, pp. 45–59 (1978).
4. M. B. Peirotti, M. D. Giavedoni and J. A. Deiber, Natural convective heat transfer in a rectangular porous cavity with variable fluid properties validity of the Boussinesq approximation, *Int. J. Heat Mass Transfer* **30**, 2571–2581 (1987).
5. V. Passeur, M. G. Satish and L. Robillard, Natural convection in the thin, inclined, porous layer exposed to a constant heat flux, *Int. J. Heat Mass Transfer* **30**, 537–549 (1987).
6. D. Poulikakos and A. Bejan, Natural convection in a porous layer heated and cooled along one vertical side, *Int. J. Heat Mass Transfer* **27**, 1879–1891 (1984).
7. V. Prasad and F. A. Kuiacki, Convective heat transfer in a rectangular porous cavity effect of aspect ratio on flow structure and heat transfer, *ASME J. Heat Transfer* **106**, 158–165 (1984).

8. V. Prasad and F. A. Kuiacki, Natural convection in a rectangular porous cavity with constant heat flux on one vertical wall, *ASME J. Heat Transfer* **106,** 152–157 (1984).
9. O. Kvernvold and P. A. Tyvand, Nonlinear thermal convection in anisotropic porous media, *J. Fluid Mech.* **90,** 609–624 (1979).
10. S. Bories, Natural convection in porous media. In *Advances in Transport Phenomena in Porous Media*, NATO ASI series. Nijhoff, Boston (1989).
11. P. J. Burns, L. C. Chow and C. L. Tien, Convection in a vertical slot filled with porous insolution, *Int. J. Heat Mass Transfer* **20,** 919–926 (1977).
12. A. Bejan and R. Anderson, Heat transfer across a vertical impermeable partition imbedded in porous medium, *Int. J. Heat Mass Transfer* **24,** 1237–1245 (1981).
13. A. Bejan, Natural convection heat transfer in a porous layer with internal flow obstruction, *Int. J. Heat Mass Transfer* **26,** 815–822 (1983).
14. T. W. Tong and E. Subramanian, Natural convection in rectangular enclosure partially filled with a porous medium, *Int. J. Heat Fluid Flow* **7,** 3–11 (1986).
15. C. Beckermann, S. Ramadhyani and R. Viskanta, Natural convection flow and heat transfer between a fluid layer and a porous layer inside a rectangular enclosure, *J. Heat Transfer* **109,** 363–370 (1987).
16. D. M. Kim and R. Viskanta, Study of the effects of conductance on natural convection in differently oriented square cavities, *J. Fluid Mechanics* **144,** 153–176 (1984).
17. S. V. Patankar, *Numerical Heat Transfer and Fluid Flow*. Hemisphere, New York (1980).
18. G. Castinel and M. Combarnous, Natural convection in an anisotropic porous layer, *Int. Chem. Engng* **17,** 605–614 (1977).
19. T. Nilsen and L. Storesletten, An analytical study on natural convection in isotropic and anisotropic porous channels, *ASEM J. Heat Transfer* **112,** 396–401 (1990).